Journal of Power Sources 195 (2010) 6699–6708

Contents lists available at ScienceDirect

Journal of Power Sources

journal homepage: www.elsevier.com/locate/jpowsour

Prediction-based optimal power management in a fuel cell/battery plug-in hybrid vehicle

Piyush Bubna, Doug Brunner, Suresh G. Advani*,[1], Ajay K. Prasad[2]

Center for Fuel Cell Research, Department of Mechanical Engineering, University of Delaware, Newark, DE 19716, United States

ARTICLE INFO

Article history:
Received 13 January 2010
Received in revised form 5 April 2010
Accepted 5 April 2010
Available online 10 April 2010

Keywords:
Fuel cell
Battery
Plug-in hybrid vehicle
Drivetrain
Simulation
Prediction-based control

ABSTRACT

A prediction-based power management strategy is proposed for fuel cell/battery plug-in hybrid vehicles with the goal of improving overall system operating efficiency. The main feature of the proposed strategy is that, if the total amount of energy required to complete a particular drive cycle can be reliably predicted, then the energy stored in the onboard electrical storage system can be depleted in an optimal manner that permits the fuel cell to operate in its most efficient regime. The strategy has been implemented in a vehicle power-train simulator called LFM which was developed in MATLAB/SIMULINK software and its effectiveness was evaluated by comparing it with a conventional control strategy. The proposed strategy is shown to provide significant improvement in average fuel cell system efficiency while reducing hydrogen consumption. It has been demonstrated with the LFM simulation that the prediction-based power management strategy can maintain a stable power request to the fuel cell thereby improving fuel cell durability, and that the battery is depleted to the desired state-of-charge at the end of the drive cycle. A sensitivity analysis has also been conducted to study the effects of inaccurate predictions of the remaining portion of the drive cycle on hydrogen consumption and the final battery state-of-charge. Finally, the advantages of the proposed control strategy over the conventional strategy have been validated through implementation in the University of Delaware's fuel cell hybrid bus with operational data acquired from onboard sensors.

1. Introduction

Fuel cells have emerged as one of the most promising candidates for fuel-efficient and emission-free vehicle power generation. In particular, proton exchange membrane fuel cells have received much attention for automotive applications due to their low operating temperature and high power density. Although the primary barrier to the commercialization of fuel cells is their high cost, there are other operational hurdles that need to be overcome. In order to improve the transient performance of fuel cells, and to recover energy through regenerative braking, fuel cells are typically paired with reversible energy storage devices such as batteries or ultracapacitors to form hybrid power-trains. Such hybrid power-trains are particularly well suited for transit applications where the average power demand is low due to frequent starts and stops of the vehicle.

The high power density of reversible storage devices (batteries, ultracapacitors) combined with their ability to supply transient power demand has facilitated a downsizing of the fuel cell stack such that it only needs to provide the average power requirement over the drive cycle, thus reducing the cost. In addition, the ability of the electrical storage system to absorb energy from regenerative braking has made the concept of hybridization more attractive. However, while the presence of multiple energy sources creates opportunities to optimize efficiency, it requires intelligent strategies to manage power flow.

Rodatz et al. [1] proposed a control strategy (equivalent consumption minimization strategy) to determine the real-time optimal power distribution. Kim and Peng [2] formulated a combined power management/design optimization approach and proposed a parameterizable and near-optimal controller for power management optimization using a stochastic dynamic programming algorithm. Paladini et al. [3] performed an optimization of vehicle configuration and control strategy to minimize hydrogen consumption while sustaining battery state-of-charge. Paladini et al. [4] have performed control strategy optimization for charge-sustaining operation of batteries and have reported good fuel economy and final battery state-of-charge (SOC) for a fuel cell/battery hybrid system. These proposed control strategies are

* Corresponding author. Tel.: +1 302 831 8975; fax: +1 302 831 3619.
E-mail addresses: advani@udel.edu (S.G. Advani), prasad@udel.edu (A.K. Prasad).
[1] George W. Laird Professor of Mechanical Engineering.
[2] Director, Center for Fuel Cell Research, University of Delaware.

0378-7753/$ – see front matter © 2010 Elsevier B.V. All rights reserved.
doi:10.1016/j.jpowsour.2010.04.008

aimed towards fuel savings for a charge-sustaining operation in Hybrid Electric Vehicles (HEVs).

This paper focuses on the energy management of a fuel cell/battery hybrid vehicle for a charge depletion operation, accounting for the limitations of both the energy sources. In addition to efficiency, the transient nature of the power load influences the fuel cell durability and its long-term performance. Kusoglu et al. [5] have shown that the proton exchange membrane can undergo compressive, plastic deformation due to hygrothermal loading, resulting in residual tensile stresses after unloading. These residual in-plane stresses in the membrane may explain the occurrence of cracks and pinholes in the membrane under cyclic loading. Pei et al. [6] have studied the effects of four different kinds of operating conditions on the fuel cell and have concluded that 56% of deterioration is due to load-change cycling and 33% due to start–stop cycling. Furthermore, frequent exposure of the cells to high voltages typical of open circuit conditions can accelerate membrane and catalyst degradation [7]. It is therefore desirable that the hybrid controller sends a stable power request to the fuel cell stack and avoids frequent load changes and multiple starts and stops of the stack.

The three main factors that affect the cycle life of a battery pack are storage conditions, charge and discharge control, and depth-of-discharge. Fast charge and discharge are inevitable when the batteries operate within an automotive drivetrain. The permissible depth-of-discharge and hence the available energy density is an important factor that decides the suitability of batteries in HEVs and Plug-in Hybrid Electric Vehicles (PHEVs). Some batteries, such as NiMH, are suitable for powering HEVs in which the energy from the fuel is used to keep the batteries charged up. In such applications the battery cycle life is conserved by cycling to shallow depths-of-discharge. This mode of operation is termed as charge sustaining. For application in plug-in hybrid vehicles, batteries must be deep-discharge, long cycle-life batteries [8]. Recent advancements in Li-ion technology have led to the development of lithium–titanate batteries which have higher energy density, more than 12,000 cycles (at 100% depth-of-discharge) and life expectancy of 20 calendar years [9] and thus are quite suitable for use in plug-in hybrids. The nickel–cadmium (NiCad) battery, if cycled to a certain shallow depth-of-discharge for a large number of cycles may not yield a storage capacity as large as that corresponding to normal discharge–charge cycles [10,11]. A phenomenon known as "memory effect" occurs due to a sudden depression of voltage as a result of highly repetitive patterns of use [11]. While the effect is completely reversible, it requires a dedicated and lengthy maintenance schedule [12]. It has therefore been found that it is best to discharge the NiCads as deeply as possible at the end of the drive cycle, followed by slow recharge to 100% state-of-charge thus reducing the need for maintenance cycles. Therefore, despite a limited cycle life (1200 cycles) this renders the NiCads suitable for use in PHEVs.

This paper describes the analysis, implementation and validation of a prediction-based power management strategy that reduces fuel consumption while managing power flow in a manner that promotes fuel cell stack life and performance, while depleting the battery to a desired state-of-charge at the end of the drive cycle. The main feature of the proposed strategy is that, if the total amount of energy required to complete a particular drive cycle can be reliably predicted, then the energy stored in the battery pack can be depleted in an optimal manner that permits the fuel cell to operate in its most efficient regime.

2. Vehicle configuration

The University of Delaware's Fuel Cell Hybrid Bus Program commenced in 2005 with the goal to research, build and demonstrate a fleet of fuel cell transit buses and hydrogen refueling stations in the state of Delaware. The first bus has been in daily service on the University of Delaware campus since 2007, and details about the analysis, operation and maintenance of this vehicle can be found in Bubna et al. [13]. The vehicle configuration used for this paper is described below. The bus was designed and constructed by Ebus, Inc. located in Downey, CA. It is a fuel cell and battery powered 22-ft bus that can hold 22 seated and 10 standing passengers. The bus is driven by a single three-phase AC induction motor that is rated for 130 kW peak and 100 kW continuous. The motor is coupled to the rear drive wheels through a single-speed chain drive and a differential. Two strings of nickel–cadmium batteries with a nominal voltage of 300 V each are connected in parallel. Each string consists of 50 monoblocks with each monoblock containing five cells. The cells are rated for a nominal charge capacity of 100 A h and the battery bank on the whole has a total energy capacity of 60 kW h. The fuel cell system consists of dual Ballard Mark9 SSL stacks, each with 110 cells rated at 19.4 kW. The hydrogen is stored in two composite high-pressure tanks located on the top of the bus. The tanks are rated for 350 bar and have a storage capacity of approximately 12.8 kg. The power-train schematic is shown in Fig. 1.

Although the fuel cell stack in the vehicle is adequately sized for transit service on the University of Delaware (UD) campus, it is too small to meet the average power requirement of certain standard drive cycles such as SC03 (supplemental drive cycle number 3 for federal test procedure) and UDDS (Urban Dynamometer Driving Schedule), for example. Enhancing the stack size would permit the simulation of these more demanding standard drive cycles. Therefore, for the purpose of simulation studies (Section 5), a dual fuel cell stack providing twice the power of the stack just described and a proportionately larger balance-of-plant are employed. The rest of the vehicle configuration is unchanged. It should be noted, however, that for demonstrating and validating the proposed power management strategy in an actual vehicle, our first bus containing the single stack was used.

The following sections describe the bus model and the LFM simulation tool that was used to evaluate the performance of the proposed power management strategy, the methodology and algorithm of the proposed strategy, LFM simulation results including a sensitivity analysis, and validation of the simulation results by an actual implementation of the proposed strategy in our first fuel cell bus.

3. Model description and simulation tool

A simulation tool called LFM (Light, Fast, and Modifiable) developed by Brown et al. [14] has been used in this study. A brief description of the fuel cell and battery model is presented in the following sections.

3.1. Fuel cell model

The current vs. voltage characteristic of the stack is obtained from actual performance data (polarization curve) logged from the fuel cell stack in the vehicle during operation. Hydrogen consumption as a function of current is given by

$$\dot{m}_{H_2} = \frac{n_{fc} M_{H_2} I_{st}}{2F} + \dot{m}_{purge} \quad (1)$$

where n_{fc} is the number of fuel cells, M_{H_2} is the molar mass of hydrogen, I_{st} is the stack current, F is the Faraday number and $\dot{m}_{purge}$ is the rate of hydrogen purge.

Amongst the fuel cell balance-of-plant components the air compressor consumes the major share of power. In the given model, the power consumption of the balance-of-plant has been modeled as the sum of a constant load and a variable compressor load, an approach also followed by Paladini et al. [3]. The compressor power

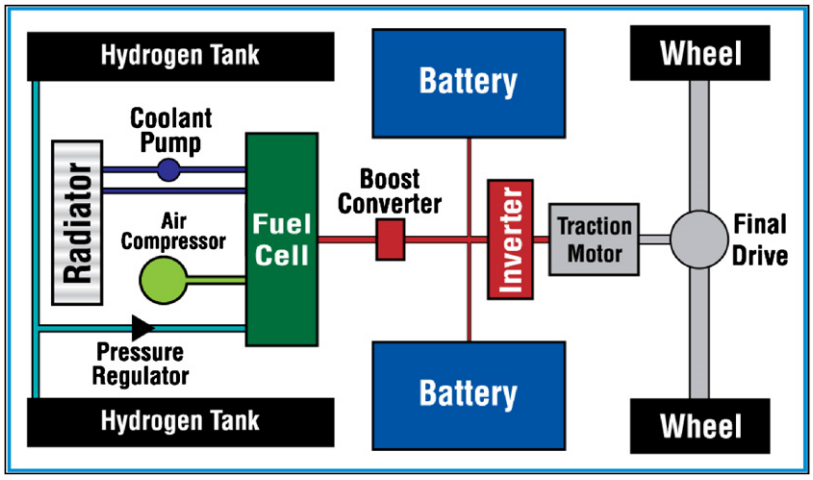

Fig. 1. Simplified schematic of the hybrid power-train.

consumption, P_{cp} depends on the stack ambient pressure ratio and the air flow rate, and is given by

$$P_{cp} = \frac{C_p T_{amb}}{\eta_m \eta_{cp}} \left[\left(\frac{p_{sm}}{p_{amb}} \right)^{(\gamma-1)/\gamma} - 1 \right] \dot{m}_{cp} \tag{2}$$

where p_{sm} is the pressure in supply manifold, p_{amb} is the ambient pressure, γ is the ratio of specific heat capacity of air at constant pressure, C_p, and the specific heat capacity of air at constant volume, C_v, T_{amb} is the ambient temperature, η_m (80%) and η_{cp} (70%) are the efficiencies of the compressor motor and compressor, respectively, and $\dot{m}_{cp}$ is the mass flow rate of air through the compressor. To predict compressor power consumption, P_{cp} as a function of stack current, a knowledge of these quantities as a function of stack current is needed. For a given stack current, I_{st}, the stoichiometric inlet oxygen mass flow rate to the cathode is given by

$$\dot{m}_{O_2,rct} = \frac{n_{fc} M_{O_2} I_{st}}{4F} \tag{3}$$

where M_{O_2} is the molar mass of oxygen. The mass flow rate of air to the cathode is given by

$$\dot{m}_{a,ca,in} = \frac{\lambda_{O_2} \dot{m}_{O_2,rct}}{y_{O_2}} = \frac{\lambda_{O_2} n_{fc} M_{O_2} I_{st}}{4 y_{O_2} F} \tag{4}$$

where λ_{O_2} is the oxygen excess ratio which is assumed to be maintained at a constant value of 1.6, and the molar fraction of oxygen in air, y_{O_2}, is 0.21. The total air flow rate through the compressor is given by

$$\dot{m}_{cp} = \dot{m}_{a,cp} + \dot{m}_{v,cp} = (1 + \psi_{amb}) \dot{m}_{a,cp} \tag{5}$$

where Ψ_{amb} is the humidity ratio of the atmospheric air, and subscripts cp, a, and v denote compressor, air, and water vapor, respectively. Also, the mass flow rate of dry air at the cathode inlet and compressor outlet can be assumed to be the same under steady state conditions. Therefore,

$$\begin{aligned} \dot{m}_{cp} &= \left(1 + \frac{M_v \phi_{amb} p_{sat,amb}}{M_a p_{a,amb}} \right) \dot{m}_{a,ca,in} \\ &= \left(1 + \frac{M_v \phi_{amb} p_{sat,amb}}{M_a p_{a,amb}} \right) \frac{\lambda_{O_2} n_{fc} M_{O_2} I_{st}}{4 y_{O_2} F} \end{aligned} \tag{6}$$

where M_a and M_v are the dry air and water vapor molar masses, respectively, φ_{amb} is the relative humidity of the ambient air (assumed to be 0.7), $p_{sat,amb}$ is the vapor saturation pressure at ambient temperature, and $p_{a,amb}$ is the pressure of the dry atmospheric air. In the vehicle p_{sm} varies from 13.5 psig to 17 psig. Based on the above analysis the gross stack power and net power can be calculated in the following way:

$$P_{fc,net} = P_{fc,gross} - P_{BOP} \tag{7}$$

$$P_{BOP} = P_{const} + P_{cp} \tag{8}$$

P_{const} is set to 1 kW for the single stack in the vehicle and P_{cp} is evaluated using Eq. (2). The plot in Fig. 2 demonstrates the gross power, net power, and balance-of-plant load as a function of stack current for the bus powered by a single stack. It should be noted that in the current implementation, the LFM simulator calculates compressor work assuming constant ambient conditions. Hence, it does not account for variations in ambient conditions that a compressor might experience during real-time operation.

The approach to reduce fuel consumption is to increase the operating efficiency of the fuel cell system which is defined as the ratio of the net power deliverable by the fuel cell to the lower heating value (LHV) of the fuel, which is hydrogen in this case.

$$\eta_{fc,sys} = \frac{P_{fc,net}}{\dot{m}_{H_2} LHV_{H_2}} \tag{9}$$

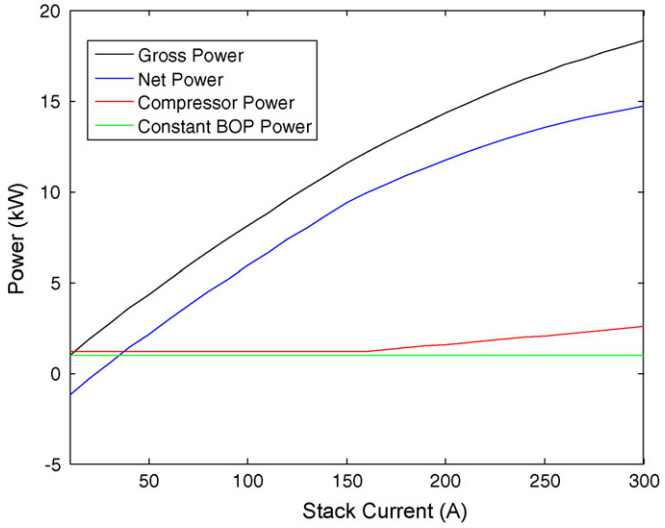

Fig. 2. Variation of gross stack power, net power, compressor power and rest of balance-of-plant load with stack current for the bus powered by a single stack.

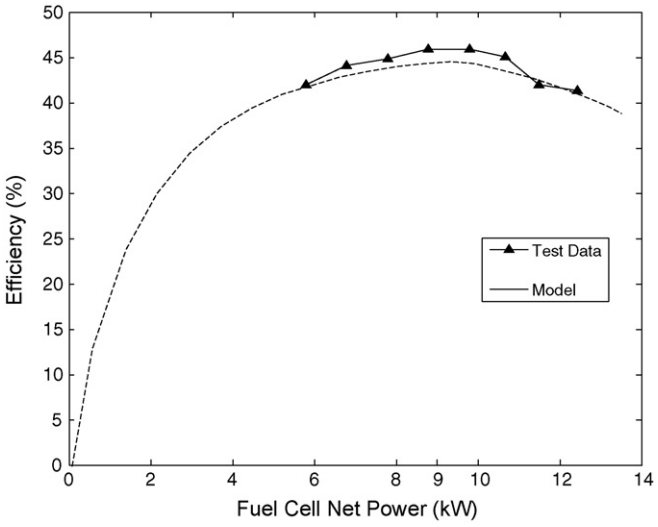

Fig. 3. Variation of fuel cell system efficiency with net fuel cell power simulated by the LFM model and the corresponding vehicle data for the bus powered by a single stack.

Similarly, the average fuel cell operating efficiency is given by

$$\eta_{fc,avg} = \frac{E_{fc,net}}{m_{H_2} LHV_{H_2}} \tag{10}$$

where $E_{fc,net}$ is the net energy delivered by the fuel cell (i.e. gross fuel cell energy minus the energy consumed by the balance-of-plant) over the duration of the drive cycle, and m_{H_2} is the corresponding total fuel consumption. The fuel cell power request is set equal to gross power. Hence it is of interest to know the variation of fuel cell system efficiency with net power. The plot of system efficiency vs. net power (Fig. 3) obtained from the above equations using parameters for the fuel cell stack in our bus reveals that the efficiency is maximized at a net power of 9 kW. Good agreement between the efficiency obtained from vehicle test data and the LFM model validates the balance-of-plant modeling approach described above. The same modeling approach is therefore extended to the dual-stack employed in the simulation studies. For the dual-stack, P_{const} is proportionately increased to 2 kW. The compressor power P_{cp} is calculated using Eq. (2). The only difference is that the dual-stack compressors are assumed to operate at lower pressures varying from 4 psig to 10 psig, assuming that an improved fuel cell stack will contain larger humidifiers. The efficiency for this system peaks at 17 kW before decreasing again at higher net power. It should be noted that the peak efficiency of the dual-stack is slightly higher than the peak efficiency of the single stack because of the reduced compressor work due to lower operating pressures.

3.2. Battery model

The NiCad battery in our buses is modeled as a voltage source in series with a resistance, both of which vary with the state-of-charge.

$$\begin{aligned} V &= V_{oc} - IR_{\text{int},dis} \quad \text{if } I > 0 \\ V &= V_{oc} - IR_{\text{int},ch} \quad \text{if } I < 0 \end{aligned} \tag{12}$$

where $V_{oc} = f(SOC)$ is the open circuit voltage of the battery pack. $R_{\text{int},dis} = f(SOC)$ and $R_{\text{int},ch} = f(SOC)$ are discharge and charge internal resistances, respectively, for both the battery strings combined. The internal resistances were obtained following Eq. (12) from OCV vs. SOC data, and voltage and current data acquired from onboard sensors during real-time transit operation of our fuel cell bus.

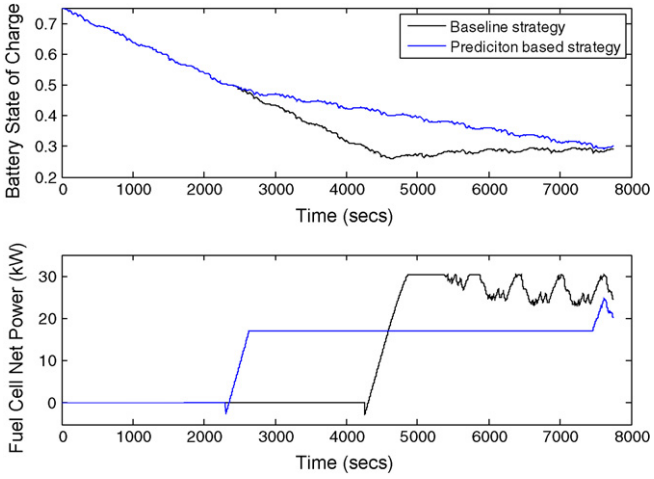

Fig. 4. Battery SOC drop and fuel cell net power corresponding to the baseline and the predictive control strategy for SC03 (~2 h, 46 miles).

$$SOC(t) = SOC_0 - \eta_{batt} \frac{\int_0^t I\,dt}{C} \tag{13}$$

where C is the charge capacity (A h) of both the strings combined, and

$$\begin{aligned} \eta_{batt} &= 1 \quad \text{if } I > 0 \text{ (discharging)} \\ \eta_{batt} &= 0.85 \quad \text{if } I < 0 \text{ (charging)} \end{aligned} \tag{14}$$

The charging reaction in NiCd chemistry is accompanied by a side reaction (electrolysis) due to which not all of the charging current goes towards converting active material. The conversion factor η_{batt} is higher at low SOCs (less electrolysis) and lower at high SOCs (more electrolysis). Based on data provided by the vehicle manufacturer, we have used an average conversion factor of 0.85 over the entire SOC range during charging. No side reactions are present during discharging and so the conversion factor is set to 1.0.

4. Power management strategy

Power flow from onboard energy sources has to be managed in order to maintain the battery SOC at a desired level. It is assumed that the battery is charged to a state of 0.75 at the start of a drive cycle in our LFM simulations. It has been observed that at SOCs higher than 0.75, the charging reaction in the NiCad battery is accompanied by the initiation of a side reaction and a limited ability to recover energy due to regenerative braking. The LFM simulator does not model this phenomenon and hence, the initial SOC is set to 0.75. Ordinarily, a charge depletion operating mode can be achieved by driving all electric until the battery is depleted to the desired SOC, followed by turning on the fuel cell system to sustain the battery at the desired SOC. This power management strategy, denoted as the baseline strategy, is depicted in Fig. 4. The following relations hold for this mode:

$$\begin{aligned} &\text{Fuel cell turn-on condition :} \quad SOC(t) \le SOC_d \\ &\text{Fuel cell power request :} \quad P(t) = P_{avg} + \alpha(SOC_d - SOC(t)) \end{aligned} \tag{15}$$

where P_{avg} is the power consumption of the traction motor and accessory load combined, averaged over a moving time frame (1 h in this case), SOC_d is the SOC to which the battery is desired to be depleted, and α is a constant in the correction term which alters the power request based on the deviation of the real-time SOC from the desired value. The value of α used in the current simulations is 600,000 W. Hence, if the SOC differential is 1% for example, then the fuel cell power request is incremented by 6 kW over P_{avg}. The

overall performance of this strategy is relatively insensitive to the value of α. For instance, the only effect resulting from a smaller α would be somewhat larger fluctuations in the subsequent time trace of SOC because the fuel cell would take longer to restore the SOC to the desired value.

Such a power management strategy suffers from a lack of control over the operating point of the fuel cell stack. For example, referring to Fig. 4, it is possible that when the fuel cell needs to be turned on, the fuel cell power request is higher than $P_{\eta_{max}}$, the value at which the fuel cell efficiency is maximized. This is because the power request to the stack is essentially governed by the average power demand of the drive cycle and the deviation of the battery SOC from the desired level. Consequently, this baseline power management strategy does not yield the highest possible fuel efficiency as the fuel cell will be operating at lower efficiency. We will use this baseline strategy as a benchmark to compare the results from the prediction-based strategy which can deliver higher efficiencies as proposed below.

Transit buses have been the most widely chosen platforms for fuel cell technology demonstration for a number of reasons as outlined in Ref. [13]. The proposed prediction-based power management strategy uses a priori knowledge of the driving route that would be typically available in transit applications and hence is particularly well suited for transit buses. This information can be exploited to manage power flow from onboard energy sources and achieve the following objectives:

- Operate the fuel cell stack in an efficient zone.
- Reduce fuel consumption.
- Send a smooth power request to the stacks and operate them without multiple starts and stops or frequent load changes.
- Discharge the battery to a desired state-of-charge at the end of the drive cycle.

4.1. Methodology and algorithm

The key to meeting the objectives stated above, is the knowledge of the expected net energy, $E_{fc,net}$, required from the fuel cell stack, which will also be referred to as the predictive parameter in this paper. This can be achieved either with the help of simulation software [14] and a priori knowledge of the drive cycle or from data acquired in real-time during an excursion of the drive cycle. Now, the ideal way to meet this energy demand is to draw net power from the fuel cell system such that the stack functions at peak efficiency. This logic is implemented in the prediction-based strategy by determining the stack turn-on time and net power request as outlined in the following algorithm. It should be noted that battery also contributes to the energy requirement of the vehicle. However, only the fuel cell energy is considered in the equations because the goal is to maximize operating efficiency of the fuel cell system.

The fuel cell stack is turned on and continues to operate the moment the following condition is met:

$$t \geq T_{cycle} - \left(\frac{E_{fc,net}}{P_{\eta_{max}}} + \delta_{corr} \right) \quad (16)$$

The power request is given by

$$\text{Power request} = \frac{E_{fc,net}}{T_{cycle} - t_{turn\,on} - \delta_{corr}} \quad (17)$$

If the battery SOC reaches SOC_d at any point during the drive cycle, the battery is operated in charge-sustaining mode for the rest of the drive cycle as has been discussed while introducing the baseline approach. The net power request and implementation condition is given by

$$\text{Power request} = P_{avg} + \alpha(SOC_d - SOC(t)) \quad \text{if } SOC(t) \leq SOC_d \quad (18)$$

where t is the current time, $t_{turn\,on}$ denotes the time when the stack is turned on, $P_{\eta_{max}}$ is the net fuel cell power corresponding to maximum system efficiency, $E_{fc,net}$ is the energy requirement from the fuel cell for the duration of the drive cycle, δ_{corr} is a correction time to start the stack earlier so as to account for the deficit in power supply during ramp up and is equal to half of the ramp up time, T_{cycle} is the total duration of the drive cycle.

The term $((E_{fc,net}/P_{\eta_{max}}) + \delta_{corr})$ denotes the time for which the stack should be operated with a net power supply of $P_{\eta_{max}}$ to meet the energy requirement $E_{fc,net}$. The conditions stated in Eqs. (16) and (17) can be understood by considering three cases that arise. They are

Case 1: $T_{cycle} > ((E_{fc,net}/P_{\eta_{max}}) + \delta_{corr})$ implies that the duration for which the stack needs to operate is less than the total duration of the drive cycle. As the drive cycle progresses, time t increases from 0 (at the start) until it reaches the value $t_{turn\,on} = T_{cycle} - ((E_{fc,net}/P_{\eta_{max}}) + \delta_{corr})$ which is when the stack turns on and continues to operate till the end of the drive cycle. Substituting for $t_{turn\,on}$ in Eq. (17) we obtain Power request $= P_{\eta_{max}}$. This is exactly the desired objective.

Case 2: $T_{cycle} = ((E_{fc,net}/P_{\eta_{max}}) + \delta_{corr})$ implies that the duration for which the stack needs to operate is equal to the duration of the drive cycle. Therefore, $t_{turn\,on} = T_{cycle} - ((E_{fc,net}/P_{\eta_{max}}) + \delta_{corr}) = 0$ and Power request $= P_{\eta_{max}}$.

Case 3: $T_{cycle} < ((E_{fc,net}/P_{\eta_{max}}) + \delta_{corr})$ implies that the duration for which the stack needs to operate is greater than the duration of the drive cycle. The earliest the stack can start is at the beginning of the drive cycle, $t = 0$. This condition is enforced by the inequality of Eq. (16). An obvious deduction is that the energy requirement $E_{fc,net}$ is met by drawing net fuel cell power which is higher than $P_{\eta_{max}}$ and is given by Eq. (17) with $t_{turn\,on} = 0$.

It should be noted that the implementation of charge-sustaining operation (Eq. (18)) ensures that the stack is operating at required power the moment the battery state-of-charge drops down to SOC_d thus safeguarding against the danger of draining the battery completely due to a delayed turn-on time, obtained from the condition specified in Eq. (16). Such a miscalculation in stack turn-on time can result from inaccurate prediction of $E_{fc,net}$ and will be discussed in the following sections.

5. Simulation results

The proposed power management strategy has been implemented in the LFM simulation software and compared with the baseline approach for drive cycles of different lengths which have been created by simply repeating the standard cycle multiple times as shown in Fig. 5. Fig. 4 demonstrates the difference between the predictive strategy and the baseline approach for the dual-stack bus. Based on the prior information of net energy requirement from the fuel cell, it can be seen that the fuel cell stack was turned on at an earlier time within the drive cycle such that the power requirement corresponds to the maximum efficiency point of the fuel cell system. The earlier start time of the stack results in a slower rate of SOC drop from the moment the stack begins to operate.

Fuel consumption, average fuel cell operating efficiency, and final battery state-of-charge are reported in Tables 1 and 2. A comparison of average fuel cell operating efficiency between the two control strategies indicates that prediction-based power management allows the stack to operate in a more efficient regime thereby reducing fuel consumption. The final battery SOC is within 3% of the desired value (0.3). The extent of fuel savings is evidently dependent upon the average operating efficiency of the fuel cell system with the baseline control strategy. For example, the aver-

Table 1
Comparison of prediction-based and baseline strategy for SC03 as shown in Fig. 5.

Drive cycle length	Output parameters	Prediction-based strategy	Baseline strategy	Fuel savings (%)
~2 h 46 miles	Hydrogen consumption (kg)	1.5855	1.8362	13.65
	Average FC system efficiency (%)	47.62	40.23	
	Final battery SOC	0.3003	0.2931	
~3 h 68 miles	Hydrogen consumption (kg)	3.1866	3.6466	12.32
	Average FC system efficiency (%)	47.71	41.29	
	Final battery SOC	0.298	0.2935	
~5 h 111 miles	Hydrogen consumption (kg)	6.4971	7.2621	10.53
	Average FC system efficiency (%)	47.03	41.85	
	Final battery SOC	0.295	0.294	
~7 h 154 miles	Hydrogen consumption (kg)	9.9537	10.8776	8.49
	Average FC system efficiency (%)	46.13	42.03	
	Final battery SOC	0.2938	0.2935	

Table 2
Comparison of prediction-based and baseline strategy for UDDS as shown in Fig. 5.

Drive cycle length	Output parameters	Prediction-based strategy	Baseline strategy	Fuel savings (%)
~2 h 45 miles	Hydrogen consumption (kg)	1.3383	1.4309	6.47
	Average FC system efficiency (%)	47.69	44.49	
	Final battery SOC	0.3033	0.3007	
~3 h 60 miles	Hydrogen consumption (kg)	2.3946	2.5724	6.91
	Average FC system efficiency (%)	47.8	44.48	
	Final battery SOC	0.3037	0.3009	
~5 h 104 miles	Hydrogen consumption (kg)	5.5909	5.9937	6.72
	Average FC system efficiency (%)	47.86	44.49	
	Final battery SOC	0.3099	0.3009	
~7 h 142 miles	Hydrogen consumption (kg)	8.292	8.8448	6.25
	Average FC system efficiency (%)	47.62	44.49	
	Final battery SOC	0.3097	0.3009	

age efficiency corresponding to the SC03 driving schedule is 41.5% as opposed to 44.5% for UDDS. This explains the relatively higher fuel savings when the new power management strategy is applied to SC03.

It should be noted that the preceding results have been generated using the same drive cycle which was also used for obtaining the parameter $E_{fc,net}$. Therefore, the predicted value of net fuel cell energy is identical to the actual value. However, in reality two realizations of the same route could lead to different drive cycles (velocity vs. time profile) due to factors that cannot be completely predicted such as instantaneous traffic conditions and ridership.

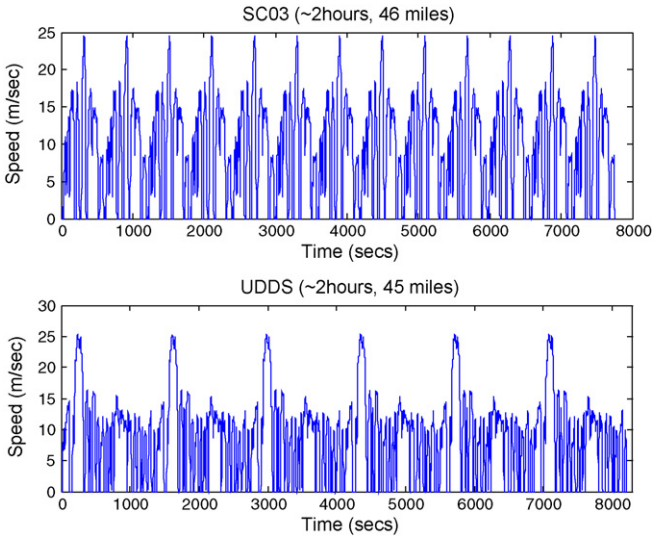

Fig. 5. Longer drive cycles formed by repeating standard cycles.

Consequently, the net energy delivered by the fuel cell stack during one excursion on a chosen route may differ from the value obtained during a different excursion on the same route. These variations can lead to an inaccuracy in the predicted parameter and its effect has been studied by means of a sensitivity analysis in the following section.

5.1. Sensitivity analysis

The inconsistency in $E_{fc,net}$ can be modeled by varying the prediction parameter corresponding to a given drive cycle and then using the modified value in the predictive control strategy for the same drive cycle. The effect of such an inaccuracy has been studied by varying the parameter by the following percentages (−15%, −10%, −5%, 5%, 10%, 15%) to reflect different degrees of inaccuracy. The modified value is then inserted into by the prediction-based strategy in order to calculate fuel cell turn-on time and determine the power request. Modifying $E_{fc,net}$ by $-x\%$ implies that we are intentionally under predicting the parameter value such that it is smaller than the correct value by $x\%$.

Modifying $E_{fc,net}$ by −15% results in under prediction of fuel cell net energy required to execute the chosen drive cycle. Consequently, the fuel cell turns on later than it should and the battery depletes to the desired SOC before reaching the destination as shown in Figs. 6 and 7. On reaching the desired SOC the strategy switches to charge-sustaining mode in accordance with the control algorithm such that the net energy supplied by the fuel cell is still equal to the original, unscaled, $E_{fc,net}$ value. However, the average operating efficiency decreases because, late in the cycle, the fuel cell is required to produce power at a higher rate at which its efficiency is lower than the maximum possible efficiency. Similarly, scaling $E_{fc,net}$ by 15% results in an over prediction of fuel cell net energy. But, unlike under prediction, in case of an over prediction,

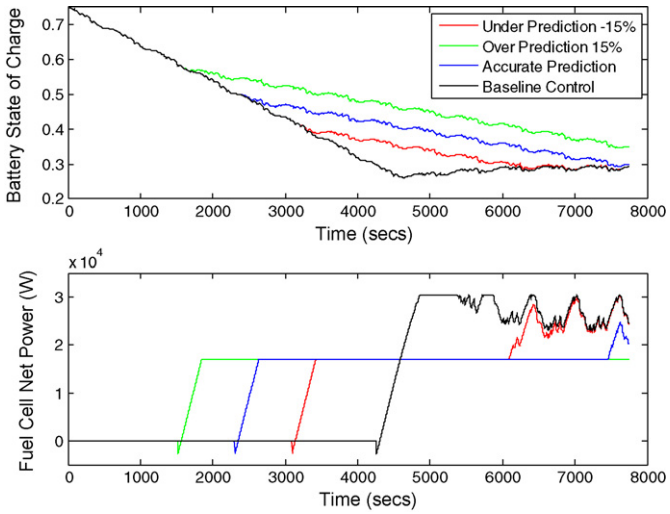

Fig. 6. Deviation in battery SOC drop and fuel cell net power corresponding to inaccuracy in prediction for the SC03 (~2 h, 46 miles).

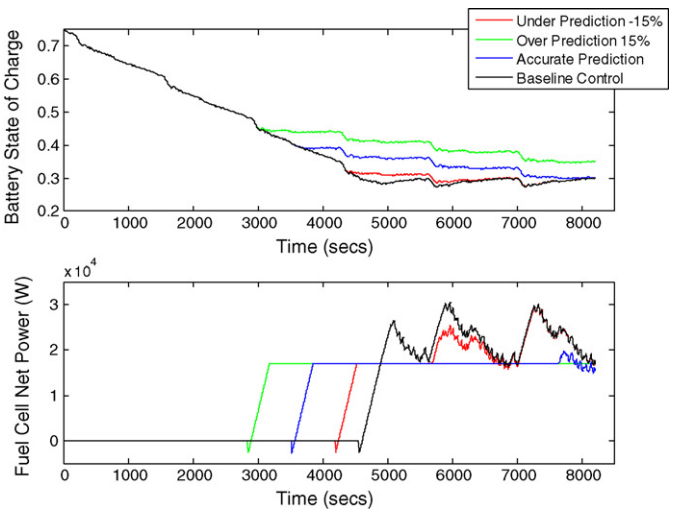

Fig. 7. Deviation in battery SOC drop and fuel cell net power corresponding to inaccuracy in prediction for the UDDS (~2 h, 45 miles).

the net energy supplied by the stack is greater than required. Consequently the terminal battery SOC stays higher than the desired SOC and fuel savings decline (Figs. 6 and 7). In both cases of inaccurate drive cycle predictions, it is of interest to analyze fuel savings with respect to the baseline control strategy which is shown in Figs. 8 and 9.

A decrease in the magnitude of fuel savings is observed for increasing degree of under prediction. For a 74 km (46 miles) SC03 drive cycle, for example, the savings are reduced to 11.39% for an under prediction of −15% as opposed to 13.65% for accurate prediction (Fig. 8). The reason, as has been stated earlier, is attributed to a decrease in average operating efficiency of the fuel cell system. A similar trend is observed for drive cycles of increasing lengths. However, the key inference from this part of study is that, the fuel savings are still positive; i.e. there is still an overall reduction in hydrogen consumption as compared to the baseline strategy while maintaining the battery SOC close to the desired level (within 3%). As expected, the magnitude of improvement diminishes with increasing amounts of under prediction.

Increasing the degree of over prediction also results in a decline in fuel savings. However, in this case, the decline occurs because the fuel cell provides more energy than what is required with the result that the battery is not discharged to the desired level. For a 74 km (46 miles) drive cycle of SC03, the terminal battery SOC is 0.35 for a 15% over prediction compared to an SOC of 0.3 for an accurate prediction (Fig. 8). For drive cycles of greater lengths the terminal battery SOC increases. This not only leads to a decrease in fuel savings, but may also result in higher fuel consumption compared to the baseline approach. Hydrogen consumption can be expected to be higher in comparison to the baseline strategy in the case of over prediction and the probability increases with the degree of over prediction and the drive cycle length.

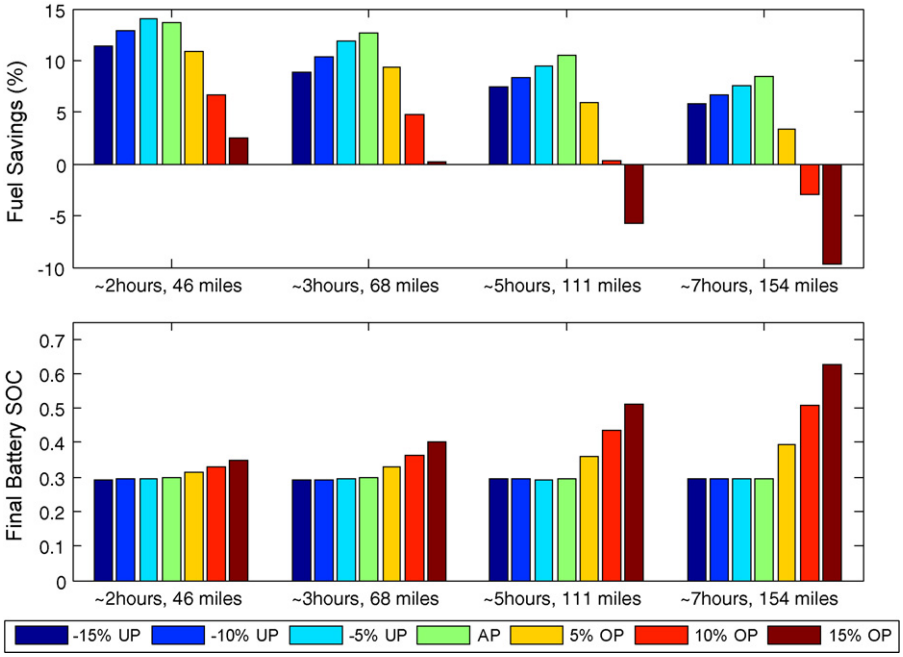

Fig. 8. Fuel savings and final battery SOC for varying degree of inaccurate predictions and for variable drive lengths for the SC03 driving schedule. UP—under prediction, AP—accurate prediction, OP—over prediction.

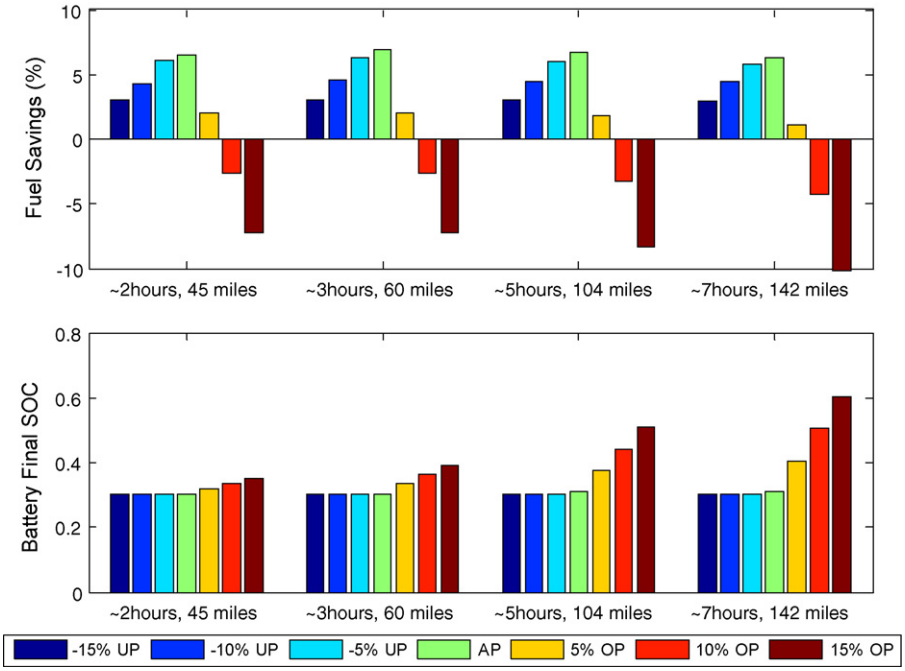

Fig. 9. Fuel savings and final battery SOC for varying degree of inaccurate predictions and for variable drive lengths for the UDDS driving schedule. UP—under prediction, AP—accurate prediction, OP—over prediction.

It should be noted that for each drive cycle considered in the present work, the average power required to sustain battery SOC, P_{avg} is greater than $P_{\eta_{\max}}$ (Fig. 3). This is expected for cost-effective power source configurations where the fuel cell is down-sized compared to the battery pack and is just enough to meet the average power requirement of urban transit drive cycles [13]. If, however, P_{avg} is less than $P_{\eta_{\max}}$, the situation always degenerates to the baseline control strategy as depicted in Fig. 10. Trajectory ADC shows the variation of SOC with time for $P_{avg} < P_{\eta_{\max}}$ if a prediction-based strategy is followed without enforcing the charge-sustaining mode at SOC_d. Evidently, the SOC reaches the desired level at B before the turn-on time at D as calculated by Eq. (16). Since it is not desirable to let the SOC fall below SOC_d, the charge-sustaining mode comes into effect at B which implies no fuel savings as the fuel cell power is below the level at which efficiency is maximized. An alternative approach, depicted by trajectory ABEC is to turn on the stack when the desired SOC is reached (at B) and draw $E_{fc,net}$ amount of energy at $P_{\eta_{\max}}$ before shutting it down (at E). In this manner, the stack can be operated at peak efficiency with additional savings in fuel.

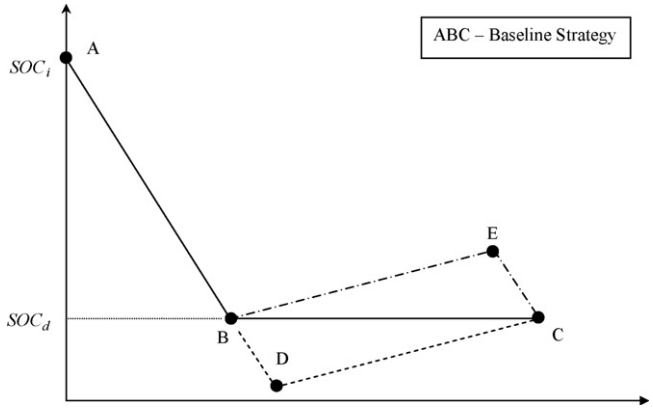

Fig. 10. Possible SOC profiles corresponding to the condition $P_{avg} < P_{\eta_{\max}}$.

6. Validation

Both the prediction-based and the baseline power management strategies were evaluated by implementing them on the University of Delaware's fuel cell/battery hybrid bus. The vehicle selected for this test was UD's first fuel cell bus; as described earlier it is equipped with a single stack rated at 19.4 kW and 60 kW h of NiCad batteries. The test was conducted by driving the bus on a defined route (Fig. 11) on two separate days, first with the baseline control strategy and next with the prediction-based strategy. During each test run the vehicle made six trips on the route and drove a total of 38.6 km (24 miles) for 100 min. The route includes two bus stops and the duration of each round trip is matched to a typical time-bound transit operation. The drive cycle (Fig. 12) includes

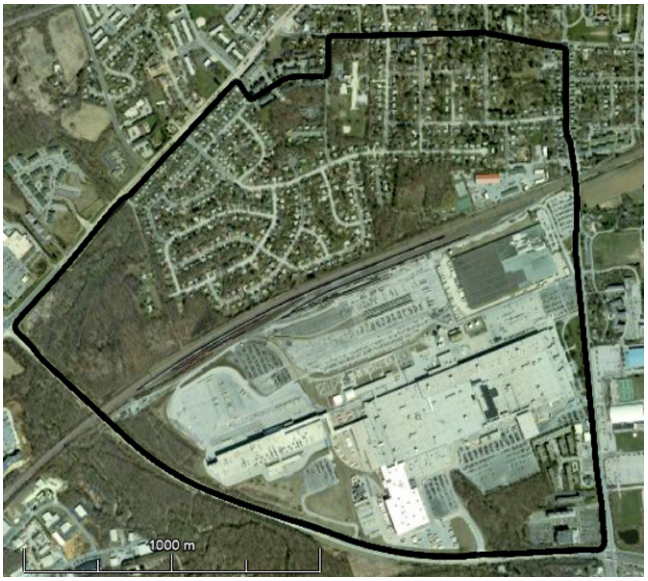

Fig. 11. Aerial view of the route followed during the test drive cycle.

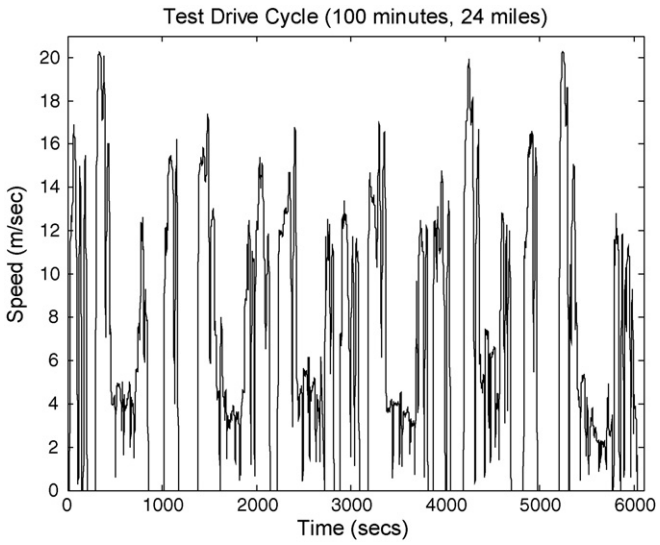

Fig. 12. Profile of the test drive cycle.

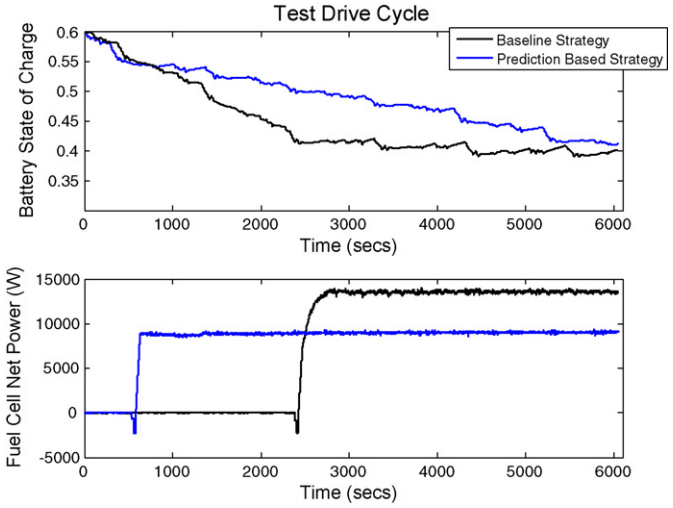

Fig. 13. Battery SOC drop and fuel cell net power corresponding to the baseline and predictive control strategies for the test drive cycle.

high and low speed segments with an average of 23.3 km h^{-1} (14.5 mph).

The initial and desired SOC were chosen to be 0.6 and 0.4, respectively, which allowed the control strategies to be tested on a drive cycle of smaller distance and duration. While operating with the baseline control strategy, the fuel cell was turned on when the SOC reached 0.41 (Fig. 13). This allowed for some warm up time so that the stack could ramp up and provide 13.5 kW of net power in order to sustain the battery at 0.4 SOC. In Fig. 12 the periodic sharp declines in SOC correspond to high power demands when the vehicle executes the high speed segment of the drive cycle. On the other hand, frequent occurrences of SOC rise are attributed to cell charging while the vehicle is idling at a bus stop or a traffic intersection. The optimal net fuel cell power of the test vehicle was obtained experimentally as 9 kW with a corresponding fuel cell system efficiency of 45.9% (Fig. 3).

The optimal power along with the net energy spent by the fuel cell during the first run (baseline strategy) was used as an input to determine the stack turn-on time for the second run that employed the prediction-based strategy. Fig. 13 shows that for the prediction-based strategy the stack turned on earlier and operated at stable optimal power for the rest of the drive cycle. A quantitative comparison of the key output parameters confirms the benefits of using the proposed power management (Table 3). Through intelligent management of energy flow and with no additional costs, the stack was operated at higher efficiency resulting in 11.7% savings in fuel consumption. Moreover, the stable operation of the fuel cell system also extends the life of the stack. The battery SOC at the end of the

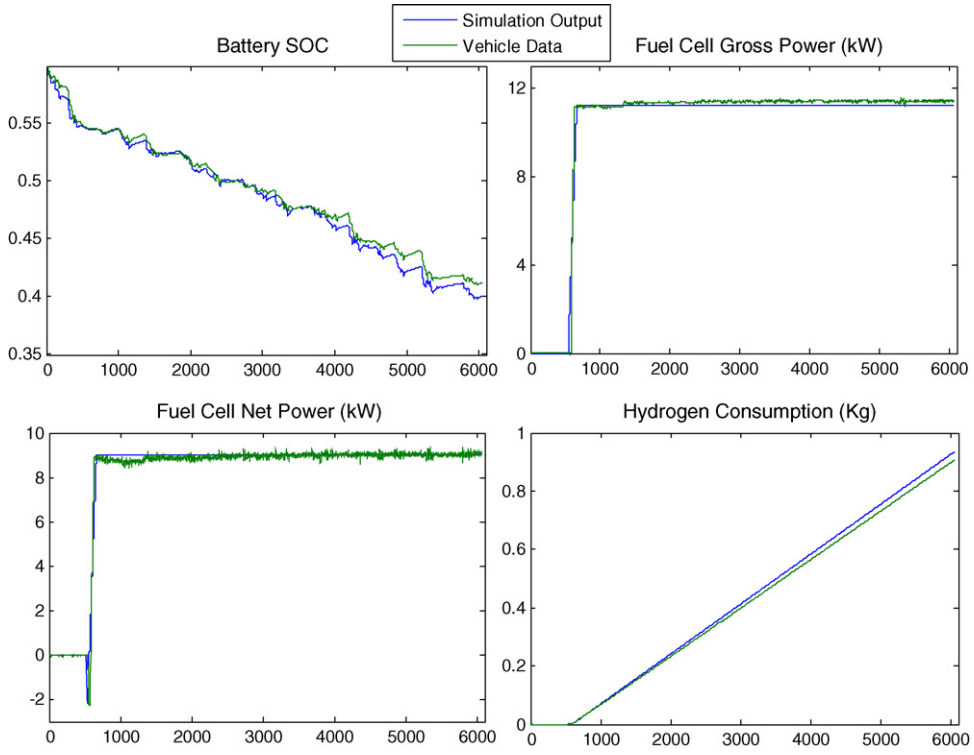

Fig. 14. Comparison of simulation output and vehicle data for the prediction-based test drive cycle.

Table 3
Comparison of prediction-based and baseline strategies for the test drive cycle.

Output parameters	Prediction-based strategy	Baseline strategy	Fuel savings (%)
Hydrogen consumption (kg)	0.9063	1.0124	11.7
Average FC system efficiency (%)	44.7	39.5	
Final battery SOC	0.4115	0.402	

Table 4
Comparison of simulation output and vehicle data for the prediction-based test drive cycle.

Output parameters	Vehicle data	Simulation output	Error (%)
Hydrogen consumption (kg)	0.906	0.934	3.1
SOC change	0.189	0.2	5.8
Battery energy (W h)	9493	10116.6	6.6
Fuel cell net energy (W h)	13503	13584	0.6
Fuel gross energy (W h)	17186	16952	1.4
Average FC system efficiency (%)	44.7	43.6	2.5

drive cycle was close to the desired lower limit, which is one of the considerations for plug-in hybrid operation.

The prediction-based power management strategy was also implemented in the LFM simulator which was customized to simulate the power-train of the test vehicle. The simulation results were found to be in good agreement with the vehicle data (Fig. 14). The fuel consumption and SOC drop given by the simulator over the entire drive cycle match very well with the actual values that were obtained from the onboard sensors in the vehicle. Table 4 quantifies the errors between the simulation output and vehicle data with respect to key parameters. The agreement between simulation output and data acquired in real-time establishes the validity of the LFM simulator used in the present study. Also, the results from the two test drives confirm the conclusions obtained from the simulations about the benefits of the prediction-based power management strategy.

7. Summary and conclusions

A new prediction-based power management strategy for fuel cell/battery plug-in hybrids has been proposed and implemented in the LFM simulation software. Simulation results for the prediction-based strategy showed significant improvements in fuel cell system efficiency and reduction in hydrogen consumption compared to a conventional, baseline strategy of charge sustenance. The importance of a stable power request to the fuel cell has been stated and realized. A sensitivity analysis was conducted to study the effects of inaccurate predictions. Results indicate that under prediction reduces the magnitude of fuel savings, and in the borderline case, may show results identical to the baseline strategy. A large degree of over prediction, on the other hand, may even lead to higher fuel consumption than the baseline strategy while resulting in a higher terminal battery SOC than desired. A conservative approach may therefore be adopted using a downscaled predicted parameter value, which results in fuel savings that may be less than the maximum possible but will safeguard against entering into the over predicted zone and the associated risk of increased fuel consumption. The implementation of the proposed strategy and its comparison with the baseline control strategy in a fuel cell and battery powered hybrid bus has confirmed the benefits predicted from simulation studies. Finally, good agreement between the simulator outputs and data acquired in real-time confirms the validity of the power-train simulator.

Acknowledgements

This research was sponsored by the Federal Transit Administration and the Delaware Department of Natural Resources and Environmental Control.

References

[1] P. Rodatz, G. Paganelli, A. Sciarretta, L. Guzzella, Control Eng. Pract. 13 (2005) 41–53.
[2] M.J. Kim, H. Peng, J. Power Sources 165 (2007) 819–832.
[3] V. Paladini, T. Danteo, A. Risi, D. Laforgia, Energy Conv. Manage. 48 (2007) 3001–3008.
[4] V. Paladini, T. Danteo, A. Risi, D. Laforgia, J. Fuel Cell Sci. Technol. 5 (2008 May).
[5] A. Kusoglu, A.M. Karlsson, M.H. Santare, S. Cleghorn, W.B. Johnson, J. Power Sources 161 (2006) 987–996.
[6] P. Pei, Q. Chang, T. Tang, Int. J. Hydrogen Energy 33 (2008) 3829–3836.
[7] A. Ohma, S. Yamamoto, K. Shinohara, Membrane degradation mechanism during open-circuit voltage hold test.
[8] A.F. Burke, Proc. IEEE 95 (April (4)) (2007).
[9] Altair Nano data sheet. Available from 2008 at www.altairnano.com.
[10] Y. Sato, K. Ito, T. Arakawa, K. Kobayakawa, J. Electrochem. Soc. 153 (October (10)) (1996).
[11] Y. Sato, S. Takeuchi, K. Kobayakawa, J. Power Sources 93 (2001) 20–24.
[12] D. Linden, Handbook of Batteries, second ed., McGraw Hill Inc., 1995.
[13] P. Bubna, D. Brunner, J.J. Gangloff Jr., S.G. Advani, A.K. Prasad, J. Power Sources 195 (2010) 3939–3949.
[14] D. Brown, M. Alexander, D. Brunner, S.G. Advani, A.K. Prasad, J. Power Sources 183 (2008) 275–281.